Self-Assembled Monolayers of Small Aromatic Disulfide and Diselenide Molecules on Polycrystalline Gold Films: A Comparative Study of the Geometrical Constraint Using Temperature-Dependent Surface-Enhanced Raman Spectroscopy, X-ray Photoelectron Spectroscopy, and Electrochemistry

Krisanu Bandyopadhyay and K. Vijayamohanan*,†

Physical/Materials Chemistry Division, National Chemical Laboratory, Pune 411008, India

M. Venkataramanan and T. Pradeep*

Department of Chemistry and Regional Sophisticated Instrumentation Centre, Indian Institute of Technology, Madras 600036, India

Received October 27, 1998. In Final Form: April 30, 1999

A detailed investigation of the self-assembled monolayers of diphenyl disulfide (DDS), diphenyl diselenide (DDSe), and naphthalene disulfide (NDS) on polycrystalline gold films using surface-enhanced Raman spectroscopy (SERS), X-ray photoelectron spectroscopy (XPS), and electrochemistry is presented. Whereas DDS dissociatively chemisorbs on Au, in both DDSe and NDS, the Se−Se and S−S bonds, respectively, are preserved upon adsorption. All of the molecules adsorb with the molecular plane perpendicular to the surface. Temperature-dependent SERS studies suggest that the DDS monolayer is by far the most stable one and is stable up to a temperature of 423 K. Both DDSe and NDS desorb without breaking the diselenide and disulfide bonds. None of the monolayers show any structural change upon heating. XPS investigations show the presence of beam-induced damage upon X-ray exposure to DDS and NDS monolayers, and the damage is greater in the latter. Electrochemical investigations support the SERS and XPS data. Number of pinholes and defects are much less in the DDS monolayer than in NDS and DDSe. The impedance parameters such as double-layer capacitance, charge-transfer resistance, and diffusion coefficients measured at different frequencies support the above conclusion. It is suggested that the geometric constraint imposed by the rigid naphthalene ring inhibits the cleavage of the S−S bond, and consequently, the adsorption sites for sulfurs are not strongly bonded. For DDSe, it appears that the Se−Se distance is such that appropriate binding sites are available, thus leading to a more ordered monolayer. For DDS, the facile cleavage of the S−S bond leads to strong binding of the adsorbate molecules at the preferred surface sites, resulting in a rather well-ordered self-assembled structure.

Introduction

Formation and the subsequent characterization of self-assembled monolayers (SAMs) have become important in the field of chemical research today[1] as self-assembly is a versatile technique for surface modification with a number of applications such as chemical sensors, nonlinear optical materials, high-density memory devices, and photopatterning methodology.[2] Although a wide variety of substrates and functional groups are known to form SAMs, the thiol/disulfide monolayer on Au has received considerable attention due to its simplicity and ease of preparation.[1] Most of the thiol/disulfide compounds investigated so far contain a long hydrophobic tail, which enables these compounds to form a compact monolayer on Au surfaces. The bonding pattern in both thiols and disulfides is the same except for an oxidative dissociation of the S−S bond for disulfides. While the nature of surface attachment is believed to involve a Au−thiolate interaction,[3] the possibility of thiolate group dimerization to form disulfides on gold surfaces has also been recently considered.[4] In contrast, selenol/diselenide monolayers have not received enough attention[5] despite their promising utility for a variety of applications such as in photoresists, photocatalysts, preparation of semiconductor quantum dots, photoinduced electron-transfer systems, and so on. More significantly, a comparison of the monolayer formation ability of the disulfides/diselenides may provide valuable information about the relative degree of organization and change in substrate−headgroup interaction with respect to the more facile nature of Se−Se cleavage.[6] DDS was selected on the basis of geometric similarity with respect to DDSe whereas NDS was used

† Phone: 0091-020-5893300. Fax: 0091-020-5893044. E-mail: viji@ems.ncl.res.in.

(1) Ulman, A. *Chem. Rev.* **1996**, *96*, 1533.

(2) (a) Hickman, J. J.; Ofer, D.; Laibinis, P. E.; Whitesides, G. M. *Science* **1991**, *252*, 688. (b) Mirkin, C. A.; Ratner, M. A. *Annu. Rev. Phys. Chem.* **1992**, *43*, 719. (c) Li, D.; Ratner, M. A.; Marks, T. J.; Znang, C. H.; Yang, J.; Wong, G. K. *J. Am. Chem. Soc.* **1990**, *112*, 7389. (d) Wollman, E. W.; Kang, D.; Frisbie, C. D.; Larcovic, T. M.; Wrighton, M. S. *J. Am. Chem. Soc.* **1994**, *116*, 4395. (e) Tariov, M. J.; Burgess, D. R. F., Jr.; Gillen, G. *J. Am. Chem. Soc.* **1993**, *115*, 5305. (f) Kawanishi, Y.; Tamaki, T.; Sakuragi, M.; Seki, T.; Swuzki, Y.; Ichimura, K. *Langmuir* **1992**, *8*, 2601.

(3) Ulman, A. *An Introduction to Ultrathin Organic Films from Langmuir−Blodgett to Self-Assembly*; Academic Press: San Diego, CA, 1991.

(4) Fenter, P.; Eberhardt, A.; Eisenberger, P. *Science* **1994**, *266*, 1216.

(5) (a) Samant, M. G.; Brown, C. A.; Gordon, J. G., II. *Langmuir* **1992**, *8*, 1615. (b) Dishner, M. H.; Hemminger, J. G.; Feher, F. J. *Langmuir* **1997**, *13*, 4788. (c) Bandyopadhyay, K.; Vijayamohanan, K. *Langmuir* **1998**, *14*, 625.

(6) Patai, S.; Rappoport, Z. *Organic Selenium and Tellurium Compounds;* John Wiley & Sons: New York, 1986; Vol. 1.

10.1021/la9815143 CCC: $18.00
Published on Web 06/24/1999

in order to reflect the role of inherent rigidity of the naphthalene ring, so that S−S bond cleavage is sterically hindered.[7]

In this paper, we study the comparative ability of SAM formation of naphthalene disulfide (NDS), diphenyl disulfide (DDS), and diphenyl diselenide (DDSe) on polycrystalline gold using surface-enhanced Raman spectroscopy (SERS), X-ray photoelectron spectroscopy (XPS), and electrochemistry. These techniques are selected on their well-proven ability to effectively unravel the molecular level details of the SAM structure[8] and the degree of organization. For example, since Raman spectroscopy can give an intense band for S−S and Se−Se stretching, valuable information could be obtained about the fate of a disulfide or diselenide bond during the monolayer formation. This aspect is important considering the *geometrical constraint* present in the NDS due to the presence of rigid naphthalene ring, which can force two sulfur atoms to a fixed distance. Most of the data obtained from different diffraction studies are consistent with a $(\sqrt{3} \times \sqrt{3})$R30° overlayer structure formed during the chemisorption of thiol/disulfide on Au (111) surfaces, and in such a model, each sulfur headgroup can occupy a 3-fold site on underlying Au (111) surface with a separation of 5 Å. Considering the constraint imposed by the naphthalene ring on two sulfurs for NDS, it is obvious that even if the S−S bond dissociates during chemisorption, the two sulfurs must retain the bonding distance of 2.4 Å (i.e., the actual S−S distance in the compound). On the contrary, DDS and DDSe will lead to two separate molecules once the S−S bond is broken. Hence, for NDS, even if one sulfur occupies the normal 3-fold hollow site, the inherent rigidity of the naphthalene ring may direct the other sulfur to a possible *quasibridge site* as the distance between a 3-fold hollow and bridge site (2.4 Å) is comparable to a S−S distance in NDS. In contrast, DDS and DDSe, free from such structural constraints, can form a normal overlayer with a S−S distance of 5 Å. The primary objective of the present investigation is to understand whether this structural difference can have any effect on the mode of organization. In addition, how the change in the headgroup from S−S to Se−Se can affect the binding mode and structure of the monolayers is also of considerable interest as organodisulfides and diselenides can also be used to organize semiconductor Q-particles of sulfides and selenides for optoelectronic applications.[9]

Experimental Section

Vacuum-deposited gold substrates with a Cr-buffer layer were prepared by previously discussed procedure.[7] All of the substrates were stored in polypropylene containers until use in order to evaluate the possibility of surface contamination during storing. Freshly evaporated Au films were also used for SAM formation. Naphthalene disulfide was prepared by the reported procedure.[10] Diphenyl disulfide, diphenyl diselenide, $K_3Fe(CN)_6$, and $K_4Fe(CN)_6$ were purchased from Aldrich and were used as received. All of the substrates were cleaned by sulfochromic acid and 3% aqueous HF followed by extensive rinsing with deionized water (Millipore system) and the solvent. After three such cleaning cycles, the substrates were blown dry by pure Argon and were immediately transferred into a deareated 1 mM solution of the specific molecule in acetonitrile. Although the monolayer formation time was varied using 12, 16, and 24 h for all three molecules, a typical time of 24 h was used for studying the SERS response. The substrates were removed after the specified time, rinsed a number of times with the solvent and finally with absolute ethanol, and then dried in a stream of Ar. All solvents were reagent grade and used without further purification. Although the above-described procedure was adequate for the measurement of reproducible X-ray photoelectron spectra, a different approach was necessary for the SERS study.

For SERS measurements, an oxidized aluminum foil of 20 μm thickness made by heating it in air at 873 K for 5 h was sputter-coated with about 2000 Å gold or silver in an Edwards sputter coater. The gold used for coating was of 99.9% purity. The films prepared this way have been shown to be excellent substrates for SERS work.[11] The films show corrugations in the submicrometer scale in scanning electron microscopy. Although sputter coating of Au on rough Al foil may not produce solely (111), this would be the preferential surface plane due to the high packing density. Even on other planes, the molecular nature of the interaction of the adsorbate with the surface is expected to be similar, and SERS results could be interpreted on the basis of adsorption on Au(111), although substrate texture in subtle ways may bring important differences in packing. All SERS measurements on these surfaces have given excellent spectra, the intensities of which were reproducible from batch to batch under identical conditions. Raman spectra were recorded with a Bruker IFS 66V FT-IR spectrometer with a FRA 106 Raman accessory. Nd:YAG laser of 1064 nm was used as the primary excitation source. A laser power of 70 mW was used. Each spectrum was an average of 500 scans, and the acquisition took nearly 30 min.

Cyclic voltammetric and impedance measurements were performed using a three electrode cell comprising of a gold-coated glass as working electrode, a large area platinum flag counter electrode, and a saturated calomel reference electrode (SCE). Cyclic voltammetry was carried out with a PAR 283 potentiostat/galvanostat and a PAR 5012 lock-in amplifier interfaced with a computer. Impedance measurements were conducted using a 5 mV rms signal at five discrete frequencies per decade. Cyclic voltammetry was performed in a solution containing only one oxidation state of the redox couple such as 1 mM $K_3Fe(CN)_6$ in 0.1 M KF. On the other hand, solutions used for impedance measurements always contained equal concentrations of the redox couple such as 5 mM $K_3Fe(CN)_6$ and 5 mM $K_4Fe(CN)_6$ in 0.5 M KF. All of the experiments were carried out at room temperature in a frequency range of 100 kHz to 0.1 Hz.

XPS measurements were performed on the SAMs using a VG Scientific ESCA LAB Mk II spectrometer operating at a pressure better than 10^{-9} Torr. The time interval between preparation of the SAM and mounting in the XPS chamber was kept to a minimum (ca. 30 min) in order to reduce any contamination. The Mg Kα induced core level spectra in the C 1s, Au 4f, O 1s, and S 2p (or Se 3p) regions were recorded at an overall instrumental resolution of ~1 eV. A large window general scan did not show the presence of any impurities. All of the binding energies (BE) were referenced to the Au $4f_{7/2}$ peak at 84 eV. During these experiments, the X-ray flux was kept low in order to reduce beam-induced damage (electron power 70 W). The peak assignments were determined by the deconvolution of experimental spectra using standard curve fitting algorithms assuming Gaussian shape.

Results and Discussions

Figure 1 shows a comparison of the normal Raman spectra of the solid samples and SER spectra of their monolayers on Au. The spectral region of 400−650 cm^{-1} in normal Raman spectra of the powder samples are especially interesting as the S−S stretching frequency lies in this region for different disulfide compounds. This region also contains a number of bands other than S−S

(7) (a) Bandyopadhyay, K.; Sastry, M.; Paul, V.; Vijayamohanan, K. *Langmuir* **1997**, *13*, 866. (b) Bandyopadhyay, K.; Patil, V.; Sastry, M.; Vijayamohanan, K. *Langmuir* **1998**, *14*, 625.

(8) (a) Joo, T. H.; Kim, K.; Kim, M. S. *J. Phys. Chem.* **1986**, 90, 5816. (b) Bryant, M. A.; Pemberton, J. E. *J. Am. Chem. Soc.* **1991**, *113*, 3629. (c) Sandhyarani, N.; Pradeep, T. *Vacuum* **1998**, *49*, 179. (d) Murty, K. V. G. K.; Venkataramanan, M.; Pradeep, T. *Langmuir* **1998**, *14*, 5446. (e) Bain, C. D.; Troughton, E. B.; Tao, Y.-T.; Evall, J.; Whitesides, G. M.; Nuzzo, R. G. *J. Am. Chem. Soc.* **1989**, *111*, 321. (f) Bain, C. D.; Evall, J.; Whitesides, G. M. *J. Am. Chem. Soc.* **1989**, 111, 7155.

(9) Gao, M.; Richter, B.; Kirstein, S. *Adv. Mater.* **1997**, *9*, 802.

(10) Gamage, S. A.; Smith, R. A. J. *Tetrahedron* **1990**, *46*, 2111.

(11) Sandhyarani, N.; Murty, K. V. G. K.; Pradeep, T. *J. Raman Spectrosc.* **1998**, *29*, 359.

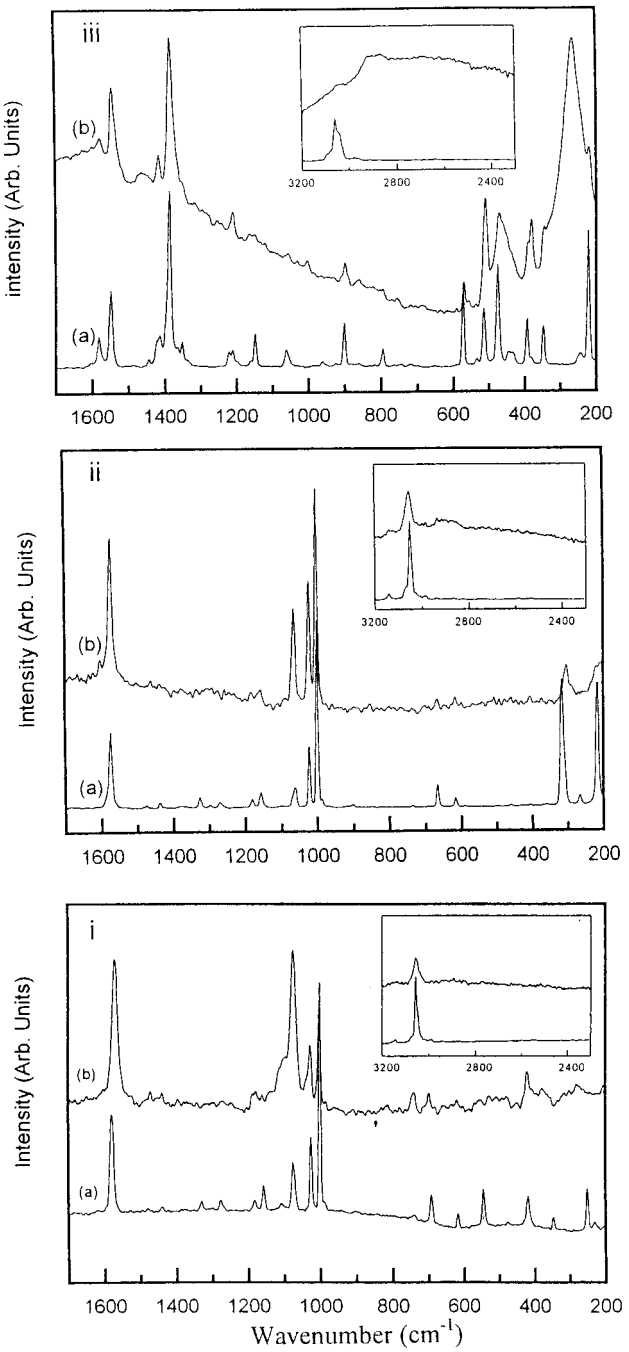

Figure 1. (a) Normal Raman and (b) SER spectra of the monolayers on Au of DDS (i), DDSe (ii), and NDS (iii). The C−H stretching region of the respective systems are shown in the inset.

stretching, possibly due to crystal field effects.[12] On the other hand, the strong Se−Se stretching vibration is known[13] to fall in the region 330−290 cm^{-1}. The S−S stretch was observed at 572 and 542 cm^{-1} for NDS and DDS, respectively, and the Se−Se stretch was seen at 310 cm^{-1}. The features observed at 416, 692, 1000, 1020, 1070, and 1572 cm^{-1} are characteristic of the benzenethio group (C_6H_5S-),[14] observed both for bulk as well as for the monolayers of DDS, DDSe, and NDS, except some difference in the last one due to the presence of naphthalene ring. It is known that for a benzene system the major peaks are ring stretch doublet near 1600 cm^{-1}, ring in-plane bending at 618 cm^{-1}, in-plane CH deformation at 1028 cm^{-1}, and in-plane ring deformation around 995 cm^{-1}.[15] In comparison, the SER spectrum of NDS, DDS, and DDSe after adsorption on the gold surface reveals several interesting features. First, it is known that disulfides can form self-assembled monolayers by an oxidative dissociation of the S−S bond, and the absence of the band at 542 cm^{-1} for DDS monolayer suggests the dissociative mode of monolayer formation.[16] In addition, the other bands due to the benzene ring are shifted to lower energy due to adsorption. Downshift of bands due to adsorption is characteristic of monolayer formation. The extent of shift is not large, indicating negligible π interaction. In contrast, 1,4-benzene dimethane thiol adsorption on Ag leads to a shift of 10 cm^{-1} for the ν_8 mode at 1600 cm^{-1}.[8c] For NDS, a band is seen at 568 cm^{-1}, suggesting the presence of undissociated S−S bonds in the adsorbed molecule. This difference in the Raman spectrum is specially significant as the probable origin of this mode can be understood in terms of the restrictions imposed by the rigid naphthalene ring. The spectrum for DDSe after adsorption on the Au surface shows a band at 301 cm^{-1}, which also indicates the possibility of the undissociated Se−Se bond. In this context, the sulfur headgroup dimerization on the Au(111) surface for long-chain thiol adsorption observed by Fenter et al.[4] is important, which contradicts the generally accepted thiolate bonding structure. In this case, the introduction of the gauche defect S−C bond allows the hydrocarbon packing to be hexagon and dimerization of the S-headgroup, which is comparable to the structural constraint in the present case. For DDSe, it appears that the Se−Se distances are such that appropriate binding sites are available leading to the undissociated diselenide bond on monolayer formation.

A comparison of normal Raman with SERS of monolayer needs some caution since the surface is not at all like those usually used to make monolayers. It is not to imply that all of the adsorbates are present with intact S−S or Se−Se bonds. Although it is difficult to quantitatively compare SERS results, useful information could be obtained for the qualitative comparison of the spectral features. For example, the SER spectra of these systems in the C−H stretching region give important information on the orientation of the adsorbed species. It has been well established that the vibrations parallel to the surface are enhanced only to a lesser extent in SERS.[17] When the benzene ring lies flat on the surface, the component of the polarizability tensor normal to the surface due to the C−H vibrations will be small, leading to a weak C−H stretching band. However, in the case of all molecules, the C−H stretching region (see the inset of Figure 1) shows peaks. Additional peaks are observed due to the combination bands in the case of NDS. This would suggest that the majority of the molecules are "sticking up" on the surface.

Variable-temperature SER spectra of the monolayers (Figure 2) reveal their comparative thermal stability. The variation of spectral features after heating the respective

(12) Van Wart, H. E.; Scherage, H. A. *J. Phys. Chem.* **1976**, *8*, 1823.
(13) Scrader, B. *Angew. Chem., Int. Ed. Engl.* **1973**, *12*, 884.
(14) Scott, P. W.; McCullough, J. P.; Hubbard, W. N.; Messerly, J. F.; Hossenlopp, I. A.; Frow, F. R.; Waddington, G. *J. Am. Chem. Soc.* **1956**, *78*, 5463.
(15) Grasselli, J. G.; Snavely, M. K.; Bulkin, B. J. In *Chemical Application of Raman Spectroscopy*; John Wiley & Sons: New York, 1976; Chapter 3.
(16) San Droff, C. J.; Herschbach, D. R. *J. Phys. Chem.* **1982**, *86*, 3277.
(17) (a) Geo, X.; Davies, J. P.; Weaver, M. J. *J. Phys. Chem.* **1990**, *94*, 6858. (b) Lee, T. G.; Kim, K.; Kim, M. S. *J. Raman Spectrosc.* **1991**, *22*, 339. (c) Kwon, C. K.; Kim, M. S.; Kim, K. *J. Raman Spectrosc.* **1989**, *20*, 575. (d) Lee, S. B.; Kim, K.; Kim, M. S. *J. Raman Spectrosc.* **1991**, *22*, 811.

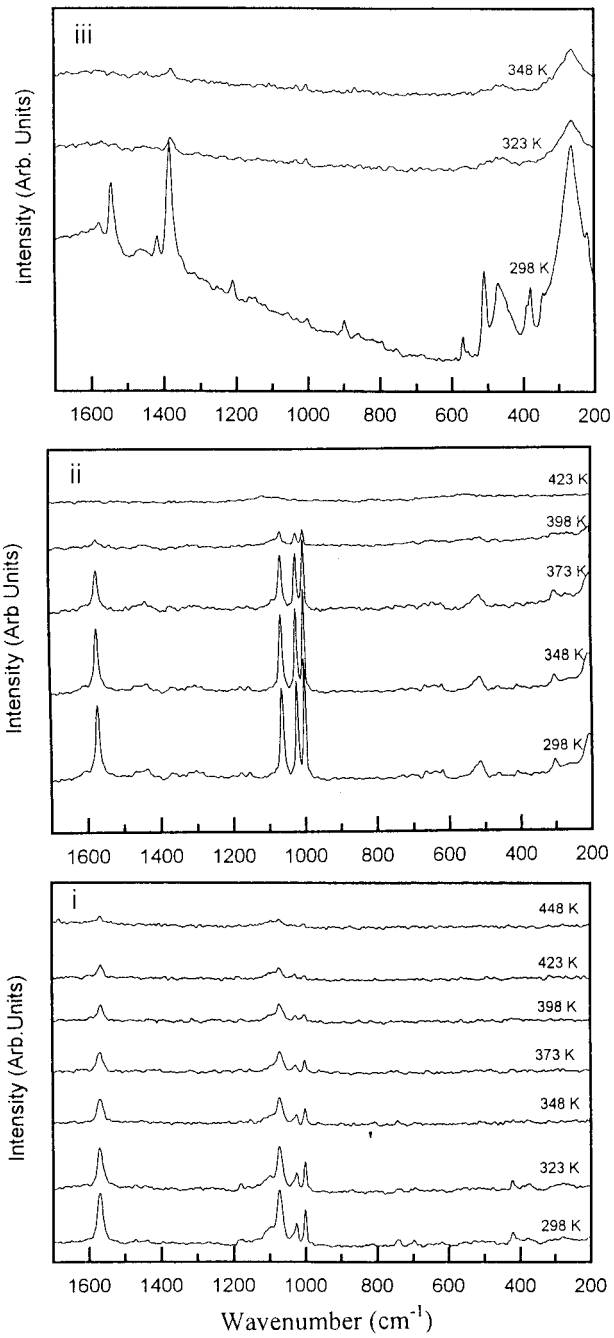

Figure 2. Temperature-dependent SER spectra of (i) DDS, (ii) DDSe, and (iii) NDS monolayers on Au. The temperatures are indicated.

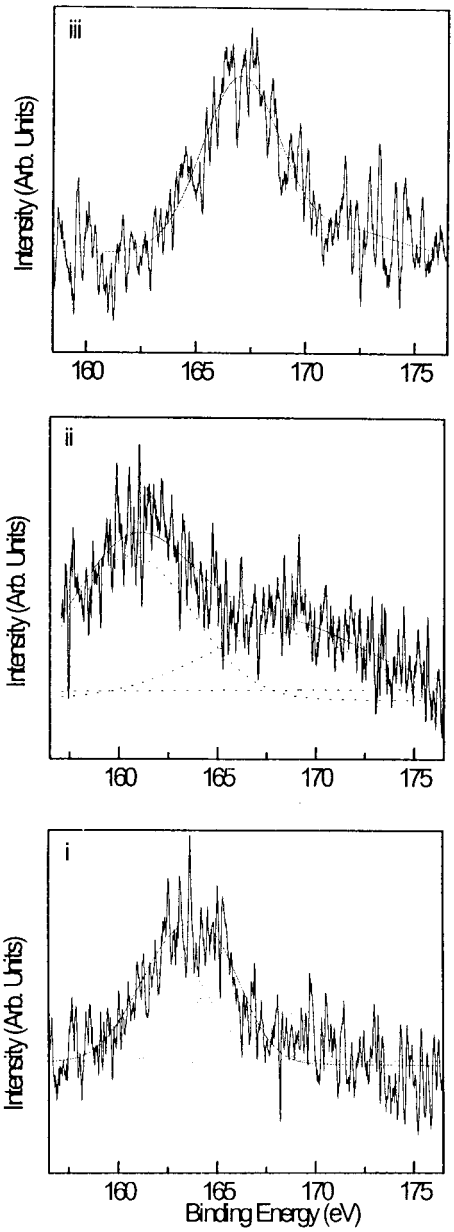

Figure 3. Mg Kα induced XP spectra of the monolayers. (i) S 2p of DDS, (ii) Se 3p of DDSe, and (iii) S 2p of NDS. Note that the DDS spectrum shows two distinct structures. The spectra have been fitted with Gaussians after background subtractions; the original data and the component peaks are shown.

samples in air from room temperature clearly shows that the intensities of major bands are totally lost at 348 K for NDS while for DDSe and DDS this happens at 423 and 448 K, respectively. This trend unambiguously suggests that the DDS monolayer on gold is thermally most stable followed by monolayers of DDSe and NDS. This order of thermal stability can be understood on the basis of the structures of the molecules and substrate−headgroup interactions. To be specific, the structure of the NDS molecule is such that it is impossible for both of the sulfurs to occupy the preferred binding sites (i.e., the normal 3-fold hollow site).[18] Therefore, for both of the sulfurs to bind the surface keeping the S−S bond intact, the hollow as well as on-top (or bridge) sites would have to take part in the bonding due to the constraint offered by the rigid naphthalene ring. On the other hand, this type of constraint is absent for DDS and DDSe, although the sulfur and selenium can have different energies of interaction with Au surface, thus explaining the different thermal stabilities.

XP spectra shown in Figure 3 (the S 2p and Se 3p binding energy values for NDS, DDS, and DDSe are listed in the Table 1) also indicate the difference in the nature of the monolayer for these three molecules on the Au surface, although only qualitative comparison is possible due to the low signal-to-noise ratio. In DDS, the S 2p peaks appear at 163.5 and 165.4 eV, the former being similar in intensity. We attribute the former to the thiolate[8e,f] (RS^-) and the latter to the X-ray beam-induced damage. Beam-induced damage in small organic thiol monolayers is well-known in the literature and leads to the formation of sulfonate or sulfate species.[8c,19] In DDSe, however, the beam-induced damage is not clearly visible. The peaks at 161.5 and 168.7

(18) Strong, L.; Whitesides, G. M. *Langmuir* **1988**, *4*, 546.

Table 1. Different Parameters Obtained for NDS, DDS, and DDSe SAMs on Gold Surface

parameters	NDS	DDS	DDSe
charge transfer resistance, R_{ct} (Ω cm^2)	567	1300	1100
apparent electrode coverage, θ (%)	99.6	99.8	99
double-layer capacitance, C (μF/cm^2)[a]	14.9	8.03	9.4
defect-free monolayer capacitance, C_s (μF/cm^2)	14.8	7.9	9.28
monolayer dielectric constant, ϵ	11.7	6.23	7.3
apparent rate constant for $Fe(CN)_6^{3-/4-}$ couple, k_{app} (cm/s)	9.3×10^{-5}	4.1×10^{-5}	2.42×10^{-4}
diffusion coefficient, D (cm^2/s)	1.2×10^{-7}	1.6×10^{-8}	4.0×10^{-8}
binding energy (eV)			
S 2p	167.2		
S 2p		163.5 and 165.4	
Se 3p			161.5 ($3p_{3/2}$)
			168.7 ($3p_{1/2}$)

[a] The double-layer capacitance of bare gold is 21 μF/cm^2 and that of octadecanethiol-modified gold is 1.4 μF/cm^2.

eV are due to $3p_{3/2}$ and $3p_{1/2}$ structures. The peaks are, however, broad, and therefore, beam-induced damage cannot be ruled out. Although there are two distinct kinds of seleniums in the monolayer (if only one is binding), they both are expected to appear within 1 eV BE. Since the Se−Se bond is retained in the monolayer, both of the atoms are expected to have more or less similar charges. In NDS, the peak is well-defined and has a substantially higher BE, and we attribute it to the beam-induced damage. It may be noted that the beam-induced oxidation is more feasible for the disordered monolayer structure.[20] Therefore, the lower intensity of the higher binding energy component for the DDS monolayer suggests a more compact and ordered monolayer structure compared to that of NDS. This conclusion from the XPS investigation can be correlated with the order of thermal stability observed in the temperature-dependent SER spectra.

XP spectra in C1s region of the monolayers are shown in Figure 4. All of the monolayer show well-defined peaks at 285 eV BE characteristic of adsorbed carbonaceous systems. Although the C1s peak position is known to depend on SAM thickness and coverage, we did not observe any such peak shift variation, perhaps due to the similarity of the molecules.[19b] In all of the samples, there were O1s peaks attributable to beam-induced damage products. No other contaminants were observed.

Electrochemical measurements, although in the presence of solvent and other ions, can be used effectively to support some of the above features of monolayer organization and coverage. For example, the differential capacity of an electrical double layer is known to decrease with increasing separation between the electrode surface and the plane of closest approach of the ionic charges.[21] Hence, double-layer capacitance studies can provide additional insights into the average structure of the self-organized assemblies. The simple parallel plate capacitance model of the electrode−electrolyte interface has been shown to be quite successful in the case of electrodes derivatized with longchain alkanethiol monolayers.[22] Our capacitance measurements at a constant potential demonstrate that NDS, DDS, and DDSe are all chemisorbed on the gold surface as manifested from the decrease in double-layer capacitance compared to that of bare gold. As the differential capacitance is extremely sensitive to the interfacial composition, these changes can be used to evaluate the extent of monolayer formation and quality.

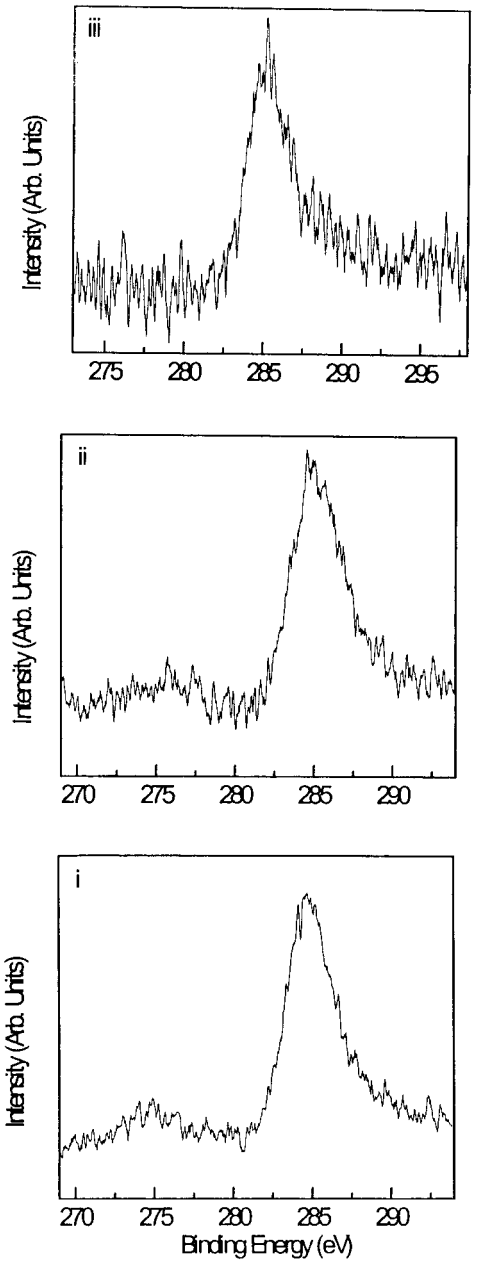

Figure 4. Mg Kα induced XP spectra of the monolayers in the C1s region: (i) DDS, (ii) DDSe, and (iii) NDS.

Figure 5 shows a plot of differential capacitance in a limited range versus applied potential in 0.1 M KF solution (pH = 7) for bare gold and gold electrodes modified with

(19) (a) Colvin, V. L.; Goldstein, A. N.; Alivisatos, A. P. *J. Am. Chem. Soc.* **1992**, *114*, 5221. (b) Ishida, T.; Hara, M.; Kojima, I.; Tsunedu, S.; Nishida, N.; Sasabe, H.; Knoll, W. *Langmuir* **1998**, *14*, 2092.

(20) Castner, D. G.; Hinds, K.; Grainger, D. W. *Langmuir* **1996**, *12*, 5083.

(21) Delahay, P. *Double Layer and Electrode Kinetics*; Interscience New York, 1965.

(22) (a) Porter, M. D.; Thomas, B. B.; Allara, D. L.; Chidsey, C. E. D. *J. Am. Chem. Soc.* **1987**, *109*, 3559. (b) Miller, C.; Cudent, P.; Grätzel, M. *J. Phys. Chem.* **1991**, *95*, 877. (c) Sabatini, E.; Rubinstein, I. *J. Phys. Chem.* **1987**, *91*, 6663.

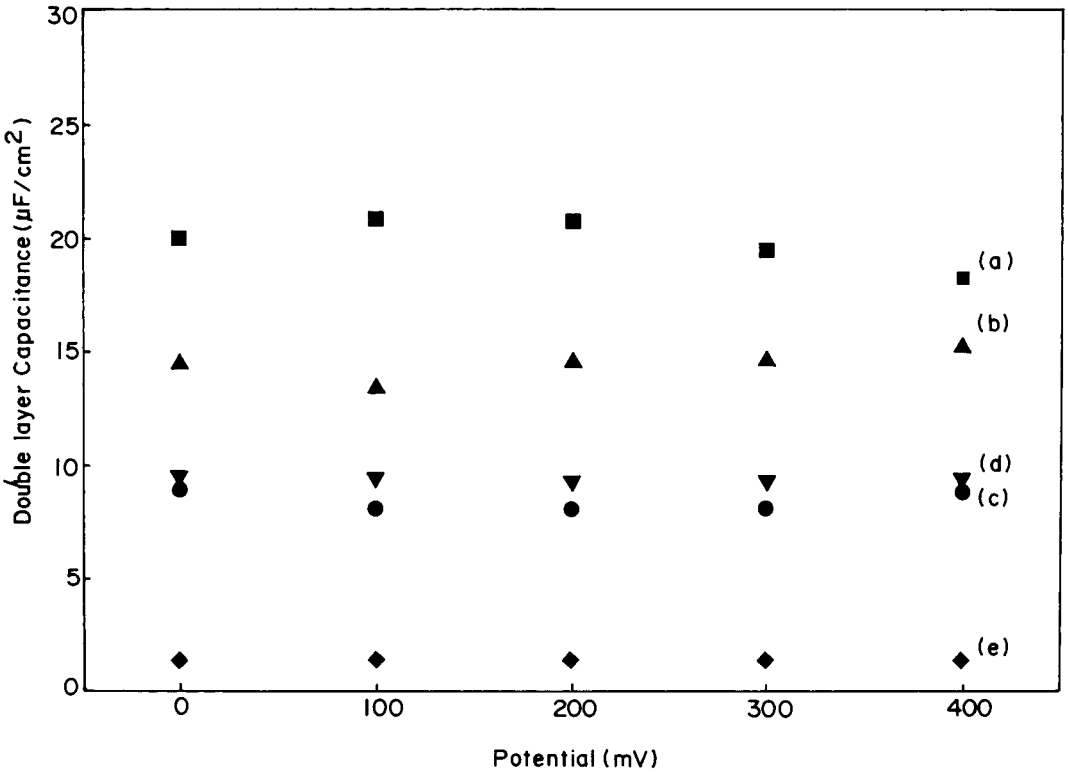

Figure 5. Variation of double-layer capacitance values with potential for (a) bare and (b) NDS-, (c) DDSe-, (d) DDS-, and (e) ODT-modified gold electrodes in 0.1 M aqueous KF.

NDS, DDS, and DDSe monolayers. These double-layer capacitance values are obtained from cyclic voltammetric data at a scan rate of 500 mV/s. The measured capacitance values are higher for both of the disulfides and the diselenide (Table 1) than those reported for compact monolayers of long-chain alkanethiols such as octadecane thiol.[22a] The higher values may be a combined effect of the presence of pinholes in the monolayer or due to the smaller molecular dimensions of the disulfides/diselenide with delocalized π-electrons. However, it should be noted that the observed double-layer capacitance values are reasonably close to the values reported in the literature[23] for such small aromatic molecules. Among the three molecules, the double-layer capacitance values are gradually increased from DDS to NDS, suggesting a greater compactness and presence of fewer pinholes in the former monolayer. The values of double-layer capacitance for DDSe indicates the poor molecular organization with the change in the headgroup from S−S to Se−Se. Monolayer formed from NDS shows the most disordered organization compared to that of the isostructural disulfide/diselenide, pointing toward the importance of structural rigidity in controlling the degree of ordering in the monolayers. The analysis of the magnitude of capacitance shows a gradual decrease from NDS to DDS monolayers, implying that more compact organization occurs for DDS. The same trend is evident in the thermal stability from SERS as well as the extent of beam-induced damage of these monolayer in XPS measurements. Among these monolayers, the double-layer capacitance value is comparatively low for DDS, indicating a greater compactness and presence of fewer pinholes.

To understand the redox activity of these molecules in solution, cyclic voltammograms have been taken in acetonitrile with 0.1 M tetrabutylammonium tetrafluoroborate as supporting electrolyte using a platinum electrode at a representative scan rate of 200 mV/s. Figure 6 shows superimposed cyclic voltammograms of all three monolayers. The voltammetric response on DDS and DDSe are similar in nature. In the case of DDSe, an irreversible oxidation peak at +1.4 V versus SCE is evident, corresponding to the formation of $C_6H_5Se^+$ from the Se−Se cleavage, along with a cathodic peak at 0.26 V. The latter cathodic peak may probably be attributed to the reduction of H^+ in the media since the electrochemical behavior of the diselenide is very similar to its sulfur analogue.[24] However, in case of the corresponding disulfide (i.e., for DDS), the oxidation peak potential is much higher (∼+1.6 V), suggesting a comparatively easy dissociation of the Se−Se over S−S bond. In comparison, voltammogram taken with a gold-coated glass as the working electrode using DDSe shows similar behavior except that the potential corresponding to cation formation has been shifted to a more positive value (+1.4 V), indicating that the formation of the cation is more favored in the case of the platinum electrode. The observed redox activity of NDS is completely different from the above-discussed disulfide and diselenide as the one-electron oxidation of the cyclic disulfide is due to the formation of a stable radical cation (an aromatic dithiolylium cation).[25] The cyclic voltammogram of the compound exhibits a reversible oxidation/reduction wave at $E_{1/2} = +0.79$ V versus SCE. The expected two-electron reduction of disulfide leading to the S−S bond cleavage is noted to be absent here. Presumably, in the monoanion, sulfur atoms are retained within the bonding distance of the rigid naphthalene backbone and further reduction is difficult due to electronic

(23) Sabatani, E.; Cohen-Boulakia, J.; Bruening, M.; Rubinstein, I. *Langmuir* **1993**, *9*, 2974.

(24) Morris, M. D.; Gregory, L. K. In *Encyclopedia of Electrochemistry of Elements*; Bard, A. J., Lund, H., Eds.; Marcel and Dekker, Inc.: New York, 1979; Vol. XIII, pp 67, 68.

(25) Chambers, J. Q. In *Encyclopedia of Electrochemistry of the Elements*; Bard, A. J., Lund, H., Eds.; Marcel Dekker Inc: New York, 1979; Vol. XII, pp 403, 406.

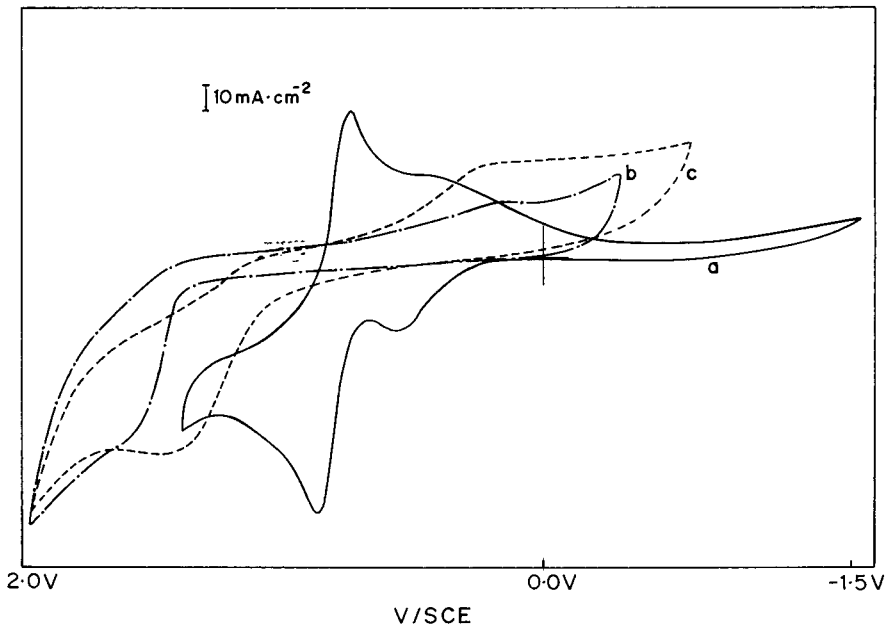

Figure 6. Superimposed cyclic voltammogram of 1 mM (a) NDS, (b) DDS, and (c) DDSe in acetonitrile with 0.1 M tetrabutylammonium tetrafluoroborate as supporting electrolyte and platinum disk as working electrode.

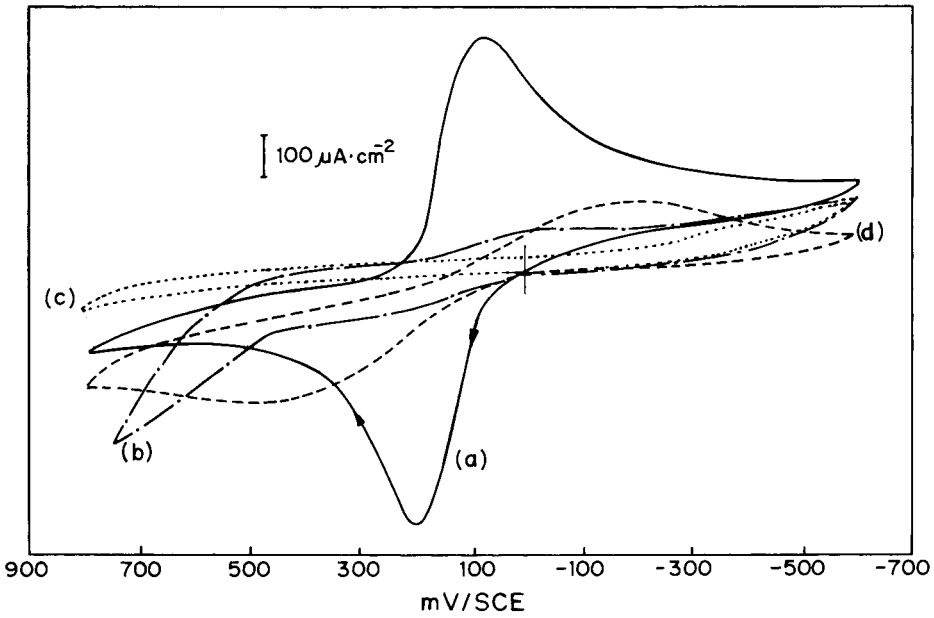

Figure 7. Superimposed cyclic voltammogram of 1 mM $K_3Fe(CN)_6$ in 0.1 M KF at (a) bare gold and (b) NDS, (c) DDS-, and (d) DDSe-modified gold electrodes after 2 h of dipping in 1 mM solution of the respective compounds in acetonitrile at a scan rate of 200 mV/s.

repulsion.[26] Further, anodic as well as the cathodic peaks in the voltammogram are not symmetric in nature, indicating the possibility of strong adsorptive interactions of both oxidized and reduced species. In addition, a response similar to surface-confined species is also indicated by the symmetrical reversible peaks around $E_{1/2} = +0.50$ V while the broadness suggests a decrease in the rate of the heterogeneous electron transfer.

Since SAM in most of the cases provides an effective barrier for the electron transfer behavior, use of external redox couple in solution can help to understand the distribution of the defect density over the monolayer. Moreover, the barrier properties can give direct microscopic evidence of the extent of molecular organization. From the superimposed cyclic voltammetric responses of the $Fe(CN)_6^{4-/3-}$ couple at bare gold-, NDS-, DDS-, and DDSe-modified electrodes shown in Figure 7, it is seen that in all of the modified electrodes the reversible response of the redox couple is not visible although a drastic reduction of the nonfaradaic current is distinct compared to the bare gold electrode. Further, among the three cases, the decrease in charging current is more for the DDS-modified electrode, suggesting that the monolayer obtained from DDS is more compact (i.e., with a smaller number of pinholes) than these obtained from NDS and DDSe. More specifically, the electron-transfer kinetics has become slower due to the barrier produced by the monolayers. Interestingly, unlike the case of long-chain thiol/disulfides, the redox activity is not totally suppressed by the monolayer here. Actually, long-chain thiols/disulfides are reported to form compact monolayers, free of

(26) Zweig, A.; Hoffmann, A. K. *J. Org. Chem.* **1965**, *30*, 3997.

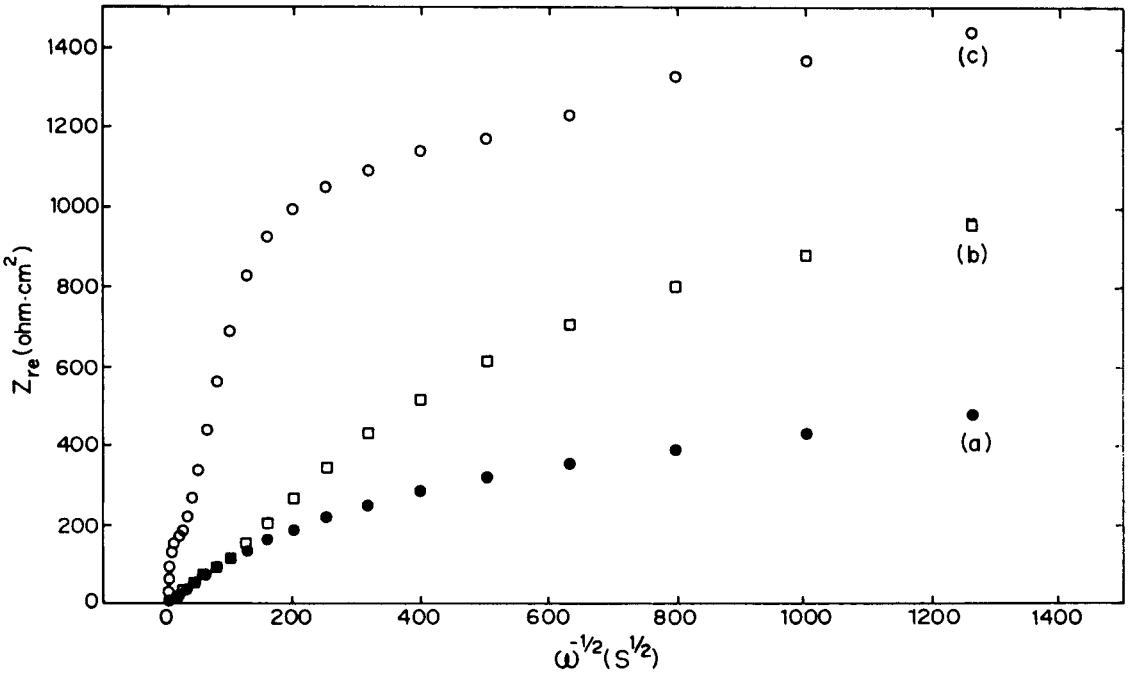

Figure 8. Superimposed plot of the real part of faradaic impedance (Z_{re}) vs $\omega^{-1/2}$ in 5 mM $K_3Fe(CN)_6$ and $K_4Fe(CN)_6$ in 0.5 M aqueous KF solution for (a) NDS monolayer, (b) DDS monolayer, and (c) DDSe monolayers on Au electrode.

measurable pinholes, which provides substantial barriers to electron transfer and strong resistance to ion penetration. The current observed at these monolayer-modified electrodes is believed to be due to electron tunneling through the long alkyl chain.[22a] On the contrary, a monolayer having a number of pinholes can show a different current−potential response depending on the distribution of the defects in the monolayer.[27] If the pinholes are close enough so that the diffusion layers overlap each other, then a current response similar to a linear diffusion is observed. On the other hand, a current response similar to a radial diffusion will be observed if the defects are small in number so that they do not overlap and hence act as an array of individual electrodes.[27] Voltammograms taken with NDS- and DDSe-modified gold electrodes indicate that the current is controlled primarily by linear diffusion as evident from the increase in peak current with the square root of the scan rate, which is unlikely for a radial mode of diffusion, in contrast to the radial mode for the DDS monolayer. The shape of the voltammograms also provides additional support for this mode of electron transfer and further suggests that the monolayer do not completely block electron transfer as these small molecules provide only a partial barrier. Moreover, the π-electrons present in the molecules can further help the electron transfer across the monolayers due to extended conjugation.

In Figure 8a−c, the real part of the faradaic impedance (Z_{re}) for NDS, DDS, and DDSe, respectively, has been plotted as a function of $\omega^{-1/2}$ after subtracting the solution resistance and interfacial capacitance from the measured total impedance. The values of uncompensated resistance and capacitance for different monolayers are obtained from the impedance data corresponding to highest frequency. The faradaic impedance plot shows features similar to those of a microarray electrode. The simulated behavior for ideal microarray electrode indicates two nearly linear domain at high and low frequencies[28] although our curves resemble more a monotonically increasing function with $\omega^{-1/2}$. This deviation from the ideal microarray behavior may be due to the nonuniform distribution of pinholes on the monolayer surface. The slope of the Z_f' versus $\omega^{-1/2}$ at the higher frequency region can also give an approximate estimate of surface coverage of the NDS and DDS monolayer using known values of the Warburg coefficient (σ).[28] The value of σ can be obtained experimentally with a bare electrode in the same solution. Analysis of Figure 8 yields θ as 0.995, 0.997, and 0.993 for NDS, DDS, and DDSe, respectively, which qualitatively suggest the compactness of all monolayers.

The analysis of the Z_f' versus $\omega^{-1/2}$ plot at lower frequency for all the monolayers shows that the slope of the curve is decreased as $\omega^{-1/2}$ is increased (with bare gold remaining constant; not shown in the figure). The Warburg coefficient (σ) calculated from the curve corresponding to each monolayer is always greater than that obtained for a bare gold electrode in the same solution. Values of σ calculated in the lower frequency region gives 216, 375, and 594 Ω cm^2/s$^{1/2}$ respectively, for NDS, DDSe, and DDS monolayers while that of bare gold is 39.5 Ω cm^2/s$^{1/2}$. The increase in the apparent value of the Warburg coefficient for monolayer-coated electrodes suggests a lower diffusion coefficient or that the pinholes are distributed in patches over the surface instead of being uniformly distributed or perhaps both.[28] Assuming equal values of diffusion coefficients for both the oxidized and reduced species, the corresponding diffusion coefficients for bare gold-, NDS-, DDS-, and DDSe-modified gold electrodes are calculated to be 3.62×10^{-6}, 1.2×10^{-7}, 1.6×10^{-8}, and 4.0×10^{-8} cm^2/s, respectively.[29] The diffusion coefficient of the bare gold electrode is in excellent agreement with the known diffusion coefficient of an aqueous solution of $Fe(CN)_6^{4-/3-}$ from independent measurements.[30] An order of magnitude reduction in the diffusion coefficient and its variation for

(27) Chailapakul, O.; Crooks, R. M. *Langmuir* **1995**, *11*, 1329.
(28) Finklea, H. O.; Snider, D. A.; Fedyk, J.; Sabatani, E.; Gafni, Y.; Rubinstein, I. *Langmuir* **1993**, *9*, 3660.

(29) This is strictly not true since bare gold offers linear semiinfinite diffusion condition whereas both modified electrodes offer a microarray diffusion condition, and this change in diffusion geometry does not allow such a comparison.
(30) Sawyer, D. T.; Roberts, J. L., Jr. *Experimental Electrochemistry for Chemists*; Wiley: New York, 1974; p 77.

the three monolayers is especially significant since the monolayers formed from DDS and DDSe allow slower ion permeation compared to that of the NDS monolayer, indicating more compact monolayer formation in the former cases.

An approximate determination of the monolayer dielectric constant is also possible from the impedance results with the help of a few additional assumptions.[22c] The C_s (double-layer capacitance value of defect-free monolayer) values (listed in Table l along with the other parameters obtained from impedance and XPS measurements) obtained can be used to calculate the dielectric permittivity of the monolayer films (ϵ_{ns}) by using the equation $\epsilon_{ns} = [C_s d]/\epsilon_o$ where d is the monolayer thickness (~7 Å) obtained from a space-filling model and ϵ_o is the permittivity of free space ($=8.85 \times 10^{-12}$ C^2 N m^{-2}). The dielectric permittivity values obtained are 11.7, 6.3, and 7.3 for NDS, DDS, and DDSe monolayers, respectively, which are in fairly good agreement with the values obtained by Rubinstein et al.[23] for *p*-biphenyl mercaptan and *p*-terphenyl mercaptan. Nevertheless, they are significantly higher compared to the values reported for pure benzene (2.28) and naphthalene (2.52),[31] indicating the importance of geometric constraints.

From a comparison of the results of SERS, XPS, and electrochemical investigations of SAMs of NDS, DDS, and DDSe on Au films, it emerges that molecular geometry as well as substrate−headgroup interaction holds a key role in determining the monolayer organization and stability. It is clearly evident that the monolayer obtained from DDS is highly organized and most stable. It undergoes less beam-induced damage and provides an effective barrier for electron transfer. Higher thermal stability of the DDS monolayer is also clear from the results of the SERS investigation. The facile S−S cleavage in DDS is the principal reason for the stability of the monolayer. Structurally similar DDSe is shown to form a monolayer which is quite stable, unlike the case of NDS which forms the thermally most unstable and least ordered monolayer, presumably due to the structural rigidity of the two sulfurs. The most interesting result is the evidence of retention of S−S and Se−Se bonds upon monolayer formation for DDSe and NDS, unlike in DDS where normal oxidative dissociation of S−S is observed.

Acknowledgment. T.P. and K.V.M. acknowledge financial support from the Department of Science and Technology, Government of India. T.P. also thanks The Jawaharlal Nehru Centre for Advanced Scientific Research and The Rajiv Gandhi Foundation. K.B. thanks the University Grants Commision, New Delhi, for a Senior Research Fellowship.

LA9815143

(31) *CRC Handbook of Chemistry and Physics*, 64 ed.; West, R., Ed.; CRC Press: Boca Raton, FL, 1984.